Effects of exhaust gas recirculation in diesel engines featuring late PCCI type combustion strategies

EFFECTS OF EXHAUST GAS RECIRCULATION IN DIESEL ENGINES FEATURING LATE PCCI TYPE COMBUSTION STRATEGIES

d'Ambrosio, S*, and Ferrari, A.

Energy Department – Politecnico di Torino

C.so duca degli Abruzzi, 24, 10129, Torino, Italy.

1. ABSTRACT

The influence of exhaust gas recirculation (*EGR*) has been analyzed considering experimental results obtained from a Euro 5 diesel engine calibrated with an optimized pilot-main double injection strategy. The engine features a late premixed charge compression ignition (*PCCI*) type combustion mode and different steady-state key-points that are representative of the engine application in a passenger car over the New European Driving Cycle (*NEDC*) have been studied. The engine was fully instrumented to obtain a complete overview of the most important variables. The pressure time history in the combustion chamber has been measured to perform calculations with single and three-zone combustion diagnostic models. These models allow the in-cylinder emissions and the temperature of the burned and unburned zones to be evaluated as functions of the crankshaft angle.

The *EGR* mass fraction was experimentally varied within the 0÷50% range. The results of the investigation have shown the influence that high *EGR* rates can have on intake and exhaust temperatures, in-cylinder pressure and heat release rate time histories, engine-out emissions (*CO*, *HC*, NO_x, soot), brake specific fuel consumption and combustion noise for a *PCCI* type combustion strategy. The outputs of the diagnostic models have been used to conduct a detailed analysis of the cause-and-effect relationships between the *EGR* rate variations and the engine performance. Finally, the effect of the *EGR* on the cycle-to-cycle variability of the engine torque has been experimentally investigated.

Keywords: exhaust gas recirculation; pollutant emissions; partial *PCCI* diesel engines.

Highlights:

- The effects that a high *EGR* rate can have on *PCCI* type combustion strategies have been analyzed.
- The dependence of engine emission and combustion noise on *EGR* has been addressed.

* Corresponding author e-mail address: stefano.dambrosio@polito.it

- The time histories of the main in-cylinder variables have been plotted for different *EGR* rates.

2. INTRODUCTION.

Conventional diesel engines are lean burning systems, if the overall air-fuel ratios are considered [1]. A premixed combustion phase is followed by a mixing-controlled combustion stage, in which the oxidation reactions are much faster than the diffusion rate of the fuel in the charge [2, 3]. Most of the fuel burns in the diffusion controlled phase and the flames are located at approximately stoichiometric regions within the overall lean, but locally inhomogeneous mixture. As a consequence, high flame temperatures, which can be estimated through adiabatic stoichiometric temperature calculations [4, 5], are obtained in the presence of oxygen and nitrogen and large amounts of NO_x are therefore generated [6, 7]. Diffusive combustion is also responsible for most of the soot generation [2] because of the presence of rich pockets within the cylinder, which cannot find the necessary oxygen amount during the later stages of combustion, especially when the engine is working at high loads [1].

External exhaust gas recirculation (*EGR*) is a strategy that is adopted in diesel engines to reduce combustion flame temperatures, which are responsible for high NO_x formation. The result of *EGR* utilization is that most of the elemental nitrogen is emitted as harmless N_2 [8-13]. Furthermore, *EGR* also has a positive effect on engine noise because it limits the heat release rate (*HRR*) during premixed combustion, which is usually characterized by rapid burning fuel [14]. However, the application of the *EGR* can determine penalties in terms of engine emissions and performance, such as particulate matter (*PM*), *CO*, unburned hydrocarbons (*HC*) and a deterioration in the brake specific fuel consumption (*bsfc*) [15-18]. In particular, extremely high values of *EGR* negatively affect the diffusive combustion process, as they increase the soot emissions and induce a rise in the cycle-to-cycle variability of combustion [1]. Nevertheless, the increase in soot generation for increasing *EGR* rates determines higher radiation and a consequent decrease in the flame temperatures that can help to further diminish NO_x emissions [8]. Finally, *EGR* can adversely affect the quality of the lubricating oil and engine durability because of increased wear between the piston rings and the cylinder liner [11, 19-21].

The benefits, with respect to the NO_x emissions, depend on the various effects induced by *EGR*: a dilution effect, a thermal effect and a chemical effect [8, 13, 22, 23]. The dilution effect of *EGR* involves a decrease in the in-cylinder oxygen concentration of the inducted charge with the main consequence of decelerating the mixing process between the injected fuel and oxygen. In addition, the quantity of inert gas that can absorb the heat release increases, and this gives rise to lower flame temperatures.

The thermal effect consists of an increase in the heat capacity of the inducted charge, because of the augmented average specific heat of the exhaust gas, which contains large amounts of CO_2 and H_2O, i.e. triatomic gases, compared to fresh

air, which mainly contains O_2 and N_2, i.e. diatomic gases. The CO_2 and H_2O concentrations in the exhaust gas are low at part loads, due to an overall leaner mixture, and, as a result, *EGR* is more effective at high loads [4, 11]. As a consequence, high *EGR* levels are required to drastically reduce the NO_x emissions at low loads [9]. Another effect, which should be included in the thermal effect of *EGR*, is due to the increase in the inlet temperature of the charge as the *EGR* rate is augmented, since the exhaust gas temperature is higher than that of fresh air. Therefore, a reduction in the charge density and in the in-cylinder trapped mass is obtained as the *EGR* rate grows under constant boost pressure. This behavior is referred to as thermal throttling [2, 8] and it determines a negative effect on NO_x reduction, since it tends to increase the maximum temperature of the burned gas, because of the higher temperature of the induced charge and roughly the same energy of the fuel absorbed by a smaller in-cylinder mass. The negative effect of thermal throttling can prevail over the beneficial thermal effect of the increased specific heat [24] in the final determination of the maximum burned gas temperature. Therefore, the utilization of cooled *EGR* is recommended [6, 25] in order to mitigate the negative effect of thermal throttling (if the cooled *EGR* temperature were the same as that of the fresh air, thermal throttling would not be present) and thus to limit the maximum in-cylinder temperature of the burned gas. The benefits of the cooled *EGR* strategy augment at high *EGR* rates, and advantages can also be observed in terms of *bsfc* and soot control [12].

The third main effect of *EGR* is of chemical nature and is due to the CO_2 and H_2O species that are present in the exhaust gas and which tend to dissociate during combustion, thus reducing the peak combustion temperature and contributing to the inhibition of NO_x formation.

When the *EGR* strategy is applied to a diesel engine, the three previously mentioned effects are present simultaneously. If a part of the oxygen content is replaced by *EGR* in the cylinder, the given amount of injected fuel has to diffuse over a wider volume before a sufficient stoichiometric mixture can be formed. The thus obtained larger stoichiometric region contains additional quantities of CO_2, H_2O and N_2, which can absorb part of the combustion-released energy and undergo dissociation phenomena, which lead to even lower flame temperatures [10, 22].

Several experiments have been performed with the purpose of evaluating the individual impact of the three abovementioned effects [8, 22]. The dilution effect is responsible for most of the NO_x reduction, and the second effect, in terms of potential, is the chemical one, while the thermal effect is generally the least important [24, 2].

As far as the influence of *EGR* on the fuel ignition delay is concerned [26, 27], the drop in the oxygen concentration, due to the dilution effect, slows down the auto-ignition reactions and enlarges the ignition delay, whereas the thermal throttling effect exerts an opposite influence [8], due to the abovementioned temperature increase of the induced charge. The dilution effect generally prevails over thermal throttling and the ignition delay therefore usually increases with the

EGR rate and allows more fuel to be evaporated and mixed with the air before combustion starts: the final result is an intensified premixed combustion mode [26].

New engine concepts related to low-temperature combustion (*LTC*), such as homogeneous charge compression ignition (*HCCI*) and partial premixed charge compression ignition (*PCCI*), are based on the utilization of large amounts of *EGR* in order to obtain a remarkable reduction in both NO_x and *PM* engine out emissions without aftertreatment systems [28], which require space, additional costs and complexities [29]. High *EGR* rates reduce peak burned gas temperatures and prolong the ignition delay, thus promoting the dispersion of the injected fuel in the charge in order to obtain highly premixed combustion. The engine *bsfc* also improves in the *LTC*, due to almost instantaneous combustion. Although *LTC* is a highly promising strategy, it is still difficult to control the combustion and to extend the strategy to the medium and high–load range of the engine [30, 31]. Furthermore, the *HC* and *CO* emissions at low engine loads represent a major concern for the low temperature combustion typology [32, 33]. In fact, the quantity of supplied fuel at light loads is small and oxidation reactions are quite slow, due to the very lean mixture and low temperatures [34]. The ignition delay is extended and this leads to increased over-mixed areas that are outside the fuel flammability limits [33]. Furthermore, retarded main injection timings, which are typical of late *PCCI* combustion strategies, further decrease peak in-cylinder temperatures. Over-mixing and bulk quenching mechanisms are considered the dominant causes of the increased *HC* and *CO* emissions in *PCCI* engines. In addition, impingement can also occur in engines managed with early *PCCI* combustion modes.

The practical implementation of the *EGR* strategy is straightforward for naturally aspirated diesel engines, because the backpressure in the exhaust tailpipe is normally higher than the intake pressure [1]. A long-route (or low-pressure) *EGR* loop [35] can be applied to turbocharged diesel engines, since a positive differential pressure is generally available between the turbine outlet and the compressor inlet. However, conventional compressors and intercoolers are not designed to endure diesel exhaust gas temperatures and high fouling levels. Therefore, the preferred solution would be to recycle the exhaust gas from upstream of the turbine to downstream of the compressor in the intake manifold, i.e. a short-route (or high-pressure) *EGR* loop would be adopted. However, this *EGR* layout is only applicable when the upstream pressure of the turbine is sufficiently higher than the boost pressure [1]. An efficient exploitation of the exhaust gas can be obtained by adopting a variable geometry turbine that can effectively provide the desired pressure level upstream of the turbine [23, 25]. In these systems, the *EGR* control is closely related to the variable geometry turbine control [36]. A very high *EGR* rate leads to an appreciable decrease in the gas flow through the turbine, and hence to a possible consequent decrease in boost pressure. For this reason, it is not feasible that a considerable reduction in NO_x could be achieved without any penalties on soot emissions for most short-route *EGR* layouts. Possible

115 improvements could be obtained by applying twin-stage turbocharger setups or by combining high-pressure and low-
116 pressure *EGR* layouts [8].
117 The present work explores the influence of cooled *EGR* mass fractions for values of up to around 50% for a Euro 5 low
118 compression ratio diesel engine, equipped with a twin-stage turbocharger and run on a late *PCCI* type combustion
119 strategy. Even though the *EGR* strategy has been studied extensively in conventional diesel engines with up to 30-40%
120 *EGR* rates [35, 37], a great deal of attention is still being paid to the effects of multiple injections in the presence of
121 heavy *EGR* rates [38, 39], which are typical of *LTC* applications. *EGR* trade-offs have been performed under different
122 steady-state working conditions that correspond to the installation of the engine on a *D*-segment vehicle that runs the
123 European emission homologation cycle. The investigation was based on experimental results obtained at the test bench.
124 Furthermore, simulations were performed using one- and three-zone combustion diagnostic models to investigate the
125 cause-and-effect relationships of the physical events.

126 ## 3. EXPERIMENTAL SET-UP.

127 The experimental tests have been carried out on the highly-dynamic test bed installed at the Politecnico di Torino
128 ICEAL (IC Engines Advanced Laboratory). The test bench was equipped with an 'ELIN AVL APA 100' cradle-
129 mounted AC dynamometer, while an 'AVL KMA 4000' with a reading accuracy of 0.1% over a 0.28-110 kg/h range
130 was used to continuously meter the fuel consumption. Furthermore, an 'AVL AMAi60' system, made up of three
131 analyzer trains, was utilized to measure the raw engine-out gaseous emissions. Two analyzer trains were equipped with
132 devices for the analysis of the *HC*, CH_4, NO_x, *CO*, CO_2 and O_2 species. The third analyzer train included a detector,
133 which was used to measure the CO_2 levels in the intake manifold, in order to evaluate the *EGR* rate. Finally, an AVL
134 415S smokemeter allowed the soot emissions in the exhaust gases to be evaluated.
135 The test engine was fully instrumented with piezoresistive pressure transducers and thermocouples in order to measure
136 the pressure and temperature in the intake, exhaust and *EGR* lines of the engine. A high-frequency piezoelectric
137 transducer was installed in the glow-plug seat to measure the pressure time-history of the gases in the combustion
138 chamber of one cylinder and one of the piezoresistive transducers was used to detect the pressure level in the inlet
139 runner of the same cylinder and thus to reference the in-cylinder pressure. All of the abovementioned measurement
140 devices are controlled by the PUMA OPEN 1.3.2 and the Indicom 1.6 automation systems.

The engine, whose main features are reported in Table 1, features a low compression ratio (16.3:1), which is in line with typical *PCCI* applications. The twin-stage turbocharger is controlled by means of two waste-gate valves. The short-route *EGR* system includes a cooled *EGR* valve on the exhaust side, which is controlled on the basis of the airflow feedback signal; a shell and tube type *EGR* cooler is placed before this valve. Furthermore, a throttle valve assembly has been placed in the intake system, downstream of the engine intercooler and just upstream of the junction with the *EGR* gases. The use of intake throttling increases the pressure drop in the *EGR* loop, and thus allows the *EGR* rate to be increased at low loads.

Engine type	2.0L Euro 5
Displacement	1956 cm^3
Bore x stroke	83.0 mm x 90.4 mm
Compression ratio	16.3
Valves per cylinder	4
Turbocharger	Twin-stage with valve actuators and waste-gate
Fuel injection system	Common Rail 2000 bar piezo
Specific power and torque	71 kW/l – 205 Nm/l

Table 1: Main specifications of the reference engine.

Key-point	SOI_{Pil} (°bTDC)	q_{Pil} (mm^3/cyl)	SOI_{Main} (° bTDC)
1500×2	11	1.7	–2
1500×5	12	1.6	–1
2000×2	16	1.5	–1
2000×5	17	1.4	0
2500×8	25	1.2	4
2750×12	31	1.1	7

Table 2: **ECU parameters for the different key-points.**

The engine was preliminarily calibrated by applying an optimized pilot-main double injection strategy, which in the present work is referred to as the baseline calibration. Steady-state tests were performed at some engine key-points, which were considered representative of the engine application to a *D*-segment passenger car over the new European driving cycle (*NEDC*). The considered key-points were expressed in terms of *n* (rpm) × *bmep* (bar) as follows: 1500×2, 1500×5, 2000×2, 2000×5, 2500×8, 2750×12.

Table 2 reports the values of the pilot injection fuel quantity per cycle and per cylinder (q_{Pil}) as well as the injection timing for both the pilot (SOI_{Pil}) and main (SOI_{Main}) injection pulses. Negative values of SOI_{Main} mean that the injection occurred after the *TDC*. The quantity of the main injection was set automatically by the test bench control system in order to maintain the desired *bmep* value. As can be inferred, the main injection timing is delayed at low loads and the pilot-to-main injection dwell times are long, in line with late *PCCI* strategies.

EGR trade-off curves were carried out at each key-point in the neighborhood of the baseline calibration point by varying the quantity of inducted air-per-cylinder and stroke, while keeping all the other engine parameters fixed.

The *EGR* mass fraction is defined as the ratio of the recirculated exhaust gas mass flow-rate to the total mass flow-rate that is inducted in the cylinder [9, 12]:

$$X_{EGR} = \frac{\dot{m}_{EGR}}{\dot{m}_{EGR} + \dot{m}_a} \quad (1)$$

where $\dot{m}_{EGR}$ and $\dot{m}_a$ are the *EGR* and fresh-air mass flow-rates, respectively. In the present investigation the calculation of X_{EGR} was performed considering the accurate expression developed in [40], which requires the evaluation of the volume concentrations of all the species at the engine exhaust and knowledge of the combustion air composition at the engine inlet. The *EGR* mass fraction can also be estimated by CO_2 volume concentration measurements in the intake manifold $[CO_2]_{int}$, and at the engine exhaust $[CO_2]_{exh}$ according to the following simplified formula, where $[CO_2]_{amb}$ represents the CO_2 volume concentration in the external environment:

$$X_{EGR} = \frac{[CO_2]_{int} - [CO_2]_{amb}}{[CO_2]_{exh} - [CO_2]_{amb}} \quad (2)$$

4. STEADY-STATE TESTS.

The *EGR* trade-off curves are plotted for the different key-points with distinct symbols, which are reported in the legend of each graph. The baseline calibration points are highlighted in each diagram with a thin line that contours the corresponding symbol.

The global air-fuel ratio, λ, is reported in Fig. 1 as a function of X_{EGR} for the different key-points. It can be observed that, for the baseline calibration key-points, the lower the load, the higher the adopted *EGR* rate: X_{EGR}≈45÷50% at the lowest load (*bmep* = 2 bar), X_{EGR}≈30÷35% at medium load (*bmep* = 5 bar) and X_{EGR}≈20÷25% at the highest loads (*bmep* = 8 and *bmep* = 12 bar). These values are higher than those usually applied in conventional diesel engines [35, 37].

The application of *EGR* limits the volume available for fresh air within the cylinder. The λ variable is generally shown to decrease almost linearly with X_{EGR} for any key-point, because the quantity of fuel is almost independent of the *EGR* mass fraction at fixed load [12]. A deviation of the λ-X_{EGR} curve from linearity can be noticed for the highest values of

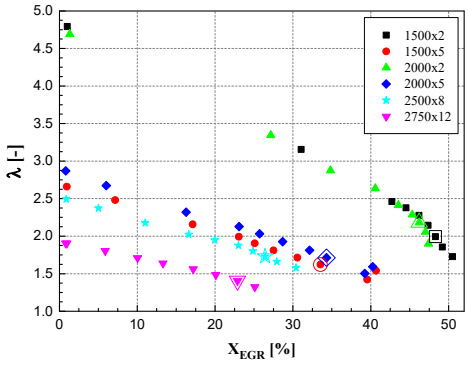

Figure 1. Relative air-fuel ratio λversus X_{EGR}

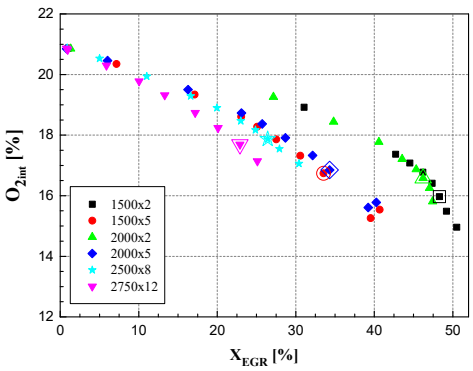

Figure 2. Oxygen volume concentration versus X_{EGR}.

X_{EGR}. In these conditions, a high mass flow-rate of gases is sent back from the engine exhaust to the intake manifold, bypassing the turbine, whereas the fresh-air flow is decreased using the intake throttle valve. As a consequence, it is not possible to maintain the desired level of boost pressure (p_{int}), which is set by the *ECU*, in the intake manifold for X_{EGR}≥40%, due to both the insufficient enthalpy flux of the exhaust gases entering the turbine and to air throttling, which reduces the pressure level in the manifold. Therefore, both the air mass flow-rate and λ decrease more than proportionally with the *EGR* mass fraction for X_{EGR}≥40%.

Figure 2 shows that an increase in X_{EGR} has a great impact on the dilution effect, because it can reduce the oxygen volume concentration $[O_2]_{int}$ in the intake manifold to a great extent, compared to the value of around 21%, which corresponds to the oxygen concentration in environmental air. In particular, *EGR* is more effective at high loads than at low loads, because the same $[O_2]_{int}$ can be obtained with a smaller X_{EGR}. In fact, as already mentioned, the CO_2 and H_2O concentrations in the exhaust gas are lower at lighter loads, since the concentrations of these species increase with the equivalence ratio $\phi=1/\lambda$. Therefore, relatively high *EGR* rates are required at low loads in order to obtain significant reductions in NO_x emissions. This explains why, the lower the load for the baseline calibration key-points in Fig. 1, the higher the X_{EGR}. In general, the load dependence of the $[O_2]_{int}$ reduction on X_{EGR} is significant, whereas the influence of the engine speed on the $[O_2]_{int}$-X_{EGR} curves is negligible.

The inlet temperature of the in-cylinder charge also rises with the *EGR* rate (Fig. 3). This produces a thermal throttling effect that occurs because the *EGR* cooler is not able to cool the recirculated exhaust gas to the same temperature as the air downstream of the intercooler. The higher the load or the speed, the higher the temperature of the gases at the engine exhaust and the higher the T_{int} temperature for a given X_{EGR} value. Thermal throttling is also induced by the increased internal residual gas fraction (internal *EGR*) that results from the growth of the exhaust manifold pressure as X_{EGR} increases. In particular, the pressure difference between the exhaust manifold and the intake manifold, which is responsible for the internal *EGR*, grows significantly for X_{EGR}≥40%, because of the intake throttle valve action.

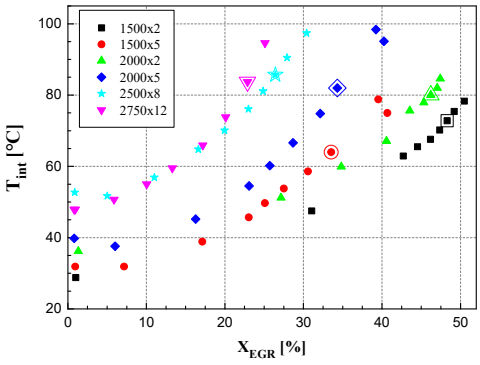

Figure 3. Engine inlet temperature versus X_{EGR}.

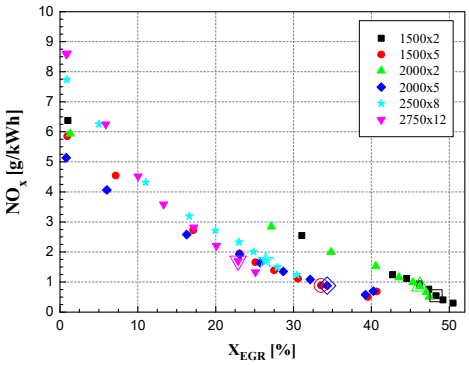

Figure 4. NO_x emissions versus X_{EGR}.

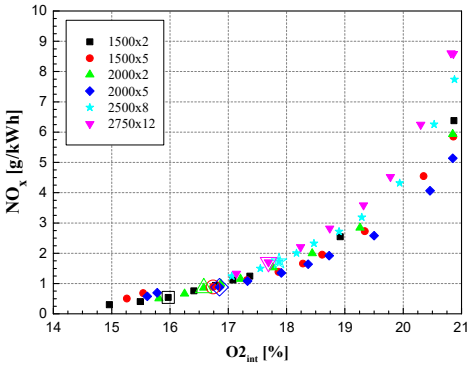

Figure 5. NO_x emissions versus O_2.

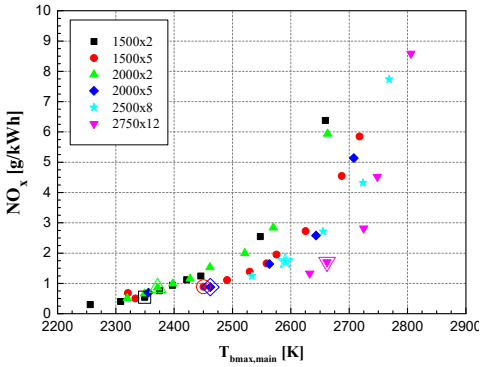

Figure 6. NO_x emissions versus $T_{bmax,main}$.

Figures 4 and 5 show the dependence of the specific NO_x emissions on the *EGR* rate and on the corresponding oxygen volume concentration in the intake manifold, respectively. Dilution is the effect that has most influence on the remarkable reduction in NO_x, as the X_{EGR} increase determines the $[O_2]_{int}$ diminution that can be observed in Fig. 5. Results, which are in agreement with those in Fig. 4, were obtained for conventional combustion mode diesel engines in [12, 18, 26] and in [27], where a reduction of approximately 50% was achieved in the NO_x emissions under $X_{EGR} \approx 20\%$ for medium load and speed. A better defined trend, which is almost independent of the specific key-point, can be seen more easily in Fig. 5 than in Fig. 4.

The reduction in the NO_x species at *bmep*=2 bar and *bmep*=5 bar is also due to the retarded main injection timing (cf. SOI_{Main} in Table 2), which postpones the combustion well into the expansion stroke. In *PCCI* type engines, retarded injection can be a complementary strategy to *EGR* for NO_x control, even though the former leads to increased fuel consumption and deteriorates *HC* emissions [11, 27].

In general, NO_x emissions are mainly affected by two factors: the presence of oxygen in the charge and the peak value of the burned-gas temperature [41]. *EGR* reduces both the oxygen volume concentration and the peak temperature of the burned gases. If the NO_x emissions are plotted as a function of the maximum burned gas temperature of the main shot (T_{bmax} has been calculated by means of a 3 zone combustion model [42]), instead of $[O_2]_{int}$, the pattern observed in Fig. 6 is achieved. However, the best correlation for NO_x is obtained with respect to $[O_2]_{int}$ in Fig. 5.

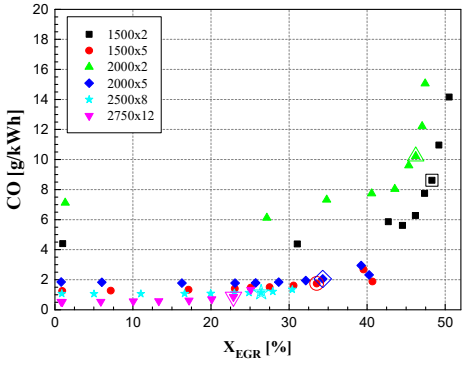

Figure 7. *HC* emissions versus X_{EGR}.

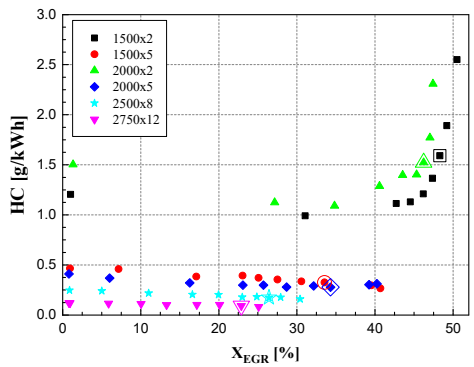

Figure 8. *CO* emissions versus X_{EGR}.

The minimum *EGR* rate that is sufficient to decrease the peak temperature of the burned gas below an acceptable threshold depends on the engine key-point and on the trade-off among different targets (i.e., the limits of different pollutant emissions set by regulations, fuel consumption and combustion noise), as well as on the synergy between combustion strategies and the aftertreatment devices installed in the exhaust pipe. The dilution, chemical and thermal effects of *EGR* simultaneously affect $T_{bmax,main}$ and it is a difficult task to properly split the contribution of each *EGR* effect during normal engine operation conditions because they occur at the same time. The calculations of the thermal properties of air and exhaust gases for the tests considered in the current investigation showed that the specific heat of the *EGR* could be up to 6% higher than the specific heat of the air, whereas the increase in the thermal capacity of the inlet charge was up to 2.5%. This variation is not able to account for the great temperature reduction in the maximum burned gas temperature that can be appreciated by considering both Figs. 4 and 6. Therefore, it can be stated that the dilution and chemical effects are more important than the thermal effect, a result that is in line with the findings in [2].

The *CO* and *HC* emissions versus X_{EGR} are plotted in Figs. 7 and 8 and show similar trends, the *CO* emissions being roughly 5 times higher than the corresponding *HC* emissions. In general, *CO* and *HC* emissions reduce as the load increases. In particular, as soon as the combustion temperature exceeds 1400-1500 K, *CO* rapidly oxidizes to CO_2 [33, 43]. The influence of the *EGR* rate on the *HC* and *CO* emissions is reduced for lower X_{EGR} values than 30%-40%, as can be seen in Figs. 7 and 8. Even the *HC* emissions exhibit a slightly decreasing trend for X_{EGR} up to 35-40% and this trend can be explained considering that the fuel can always find enough air to burn for low X_{EGR} values. As a consequence, the dilution effect of *EGR*, which impacts negatively on *HC* emissions, becomes negligible, while the thermal throttling effect of *EGR* (Fig. 3), which can promote *HC* oxidation, plays a decisive role. *HC* and *CO* emissions increase to a great extent for higher *EGR* mass fractions than 40%, as can be seen in Figs. 7 and 8, due to incomplete combustion. In fact, even though the global λ continues to be lean, the mixture is inhomogeneous and, locally, some fuel cannot find the necessary quantity of air. However, if the turbocharger can provide a sufficiently increased boost pressure, in order to

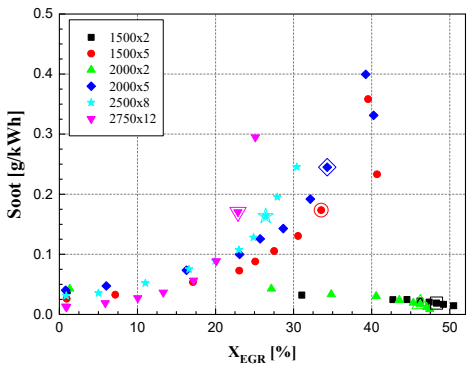

Figure 9. Soot emissions versus X_{EGR}.

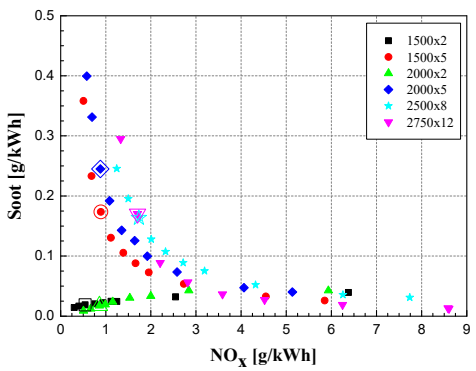

Figure 10. NO_x-soot curve as X_{EGR} varies.

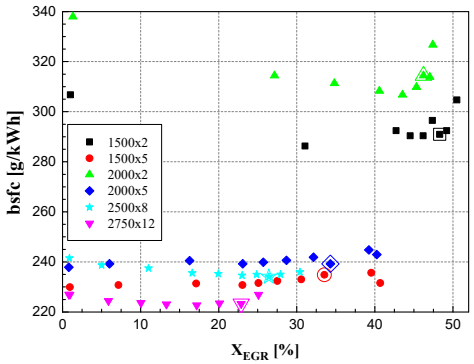

Figure 11. Brake specific fuel consumption versus X_{EGR}.

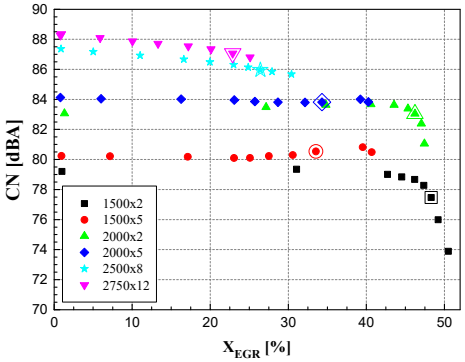

Figure 12. Combustion noise versus X_{EGR}.

maintain adequate local ϕ values, the combustion deterioration will practically be negligible. Therefore, almost similar reductions in NO_x as those shown in Fig. 5 would be achieved, but with minor increases in the *CO* and *HC* emissions. Soot emissions versus X_{EGR} are plotted in Fig. 9, where different trends, with respect to the *EGR* rate, can be observed on the basis of the considered load [15]. At the lowest loads (*bmep* = 2 bar), the soot emissions decrease as X_{EGR} increases, but, when the load is increased, it is difficult to employ high *EGR* rates, due to the deterioration in diffusive combustion, which makes the engine generate more smoke. This sensitivity of soot to *EGR* at medium and high loads is consistent with the data in [39]. Therefore, a trade-off limit must be set for X_{EGR} at medium and high loads in order to obtain a suitable compromise between NO_x and soot emissions; from this point of view, a high injection pressure or swirl ratio can also be used to suppress soot and allow the *EGR* limit to be raised [38]. Fig. 10 reports the NO_x-soot trade off curves that are obtained for *bmep* = 5 bar, *bmep* = 8 bar and *bmep* = 12 bar by varying X_{EGR}. An increase in X_{EGR} has a positive influence on both NO_x and soot emissions at *bmep* = 2 bar, since the engine works in the *PCCI* regime. However, if the engine is not run under a *PCCI* type strategy, the presence of the NO_x-soot *EGR* trade-off also persists at low loads [44]. This topic will be dealt with in more detail in section 5, where the in-cylinder analysis is presented.

Figure 11 reports *bsfc* as a function of X_{EGR} for different *bmep* values. A decrease in *bsfc* can be found when passing from no *EGR* to around X_{EGR}≈30% at *bmep* = 2 bar. This is related to the combustion of the unburned hydrocarbons that enter the combustion chamber with the recirculated exhaust gas [11]. In fact, the exhaust gas contains more O_2 at *bmep* = 2 bar than at higher loads. Furthermore, as already mentioned, cooled *EGR* acts as a pre-heater of the intake mixture.

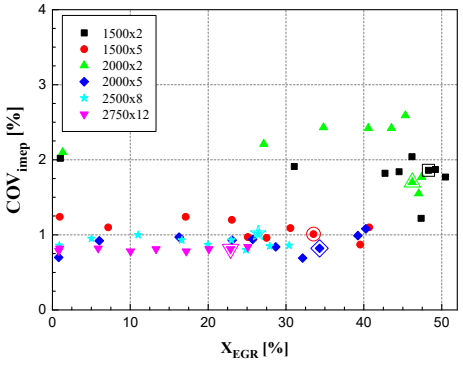

Figure 13. COV_{imep} versus X_{EGR}.

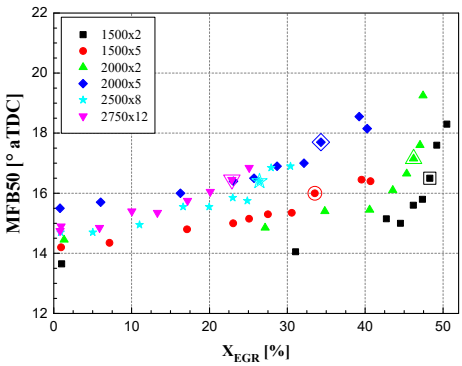

Figure 14. Combustion phasing versus X_{EGR}.

When the exhaust gas is recirculated to the cylinder inlet at a low load, the unburned *HC* in the exhaust gas burn because sufficient O_2 is available in the combustion chamber and the intake temperatures are relatively high. However, *bsfc* increases with X_{EGR} for heavy *EGR* rates and *bmep* = 2 bar, as there is not enough fresh air to burn all the injected fuel, and this represents a drawback for the use of *EGR* rates beyond $X_{EGR}\approx 40\%$. *bsfc* is less affected by the *EGR* rate at medium and high loads. The influence of *EGR* on the *bsfc* for $bmep \geq 5$ bar does not show a definite trend up to $X_{EGR}\approx 20\%$. A small increase in *bsfc* can be observed for higher *EGR* mass fractions than 20%, mainly due to the reduction in λ and to the longer duration of combustion.

Figure 12 plots the combustion noise (*CN*) as a function of X_{EGR}. The influence of *EGR* at *bmep* = 2 bar and *bmep* = 5 bar, is virtually negligible up to $X_{EGR}\approx 45\%$, whereas an important decrease in *CN* can be found for $X_{EGR}>45\%$ at *bmep*=2 bar. A continuously decreasing trend can be detected at higher loads, i.e. *bmep* = 8 bar and *bmep* = 12 bar, for $X_{EGR}\leq 30\%$.

Combustion stability is not affected to any great extent by the *EGR* rate, since the coefficient of variation of *imep* (COV_{imep}) is always lower than 3%, as can be seen in Fig. 13, and no well-defined trend of COV_{imep} with respect to X_{EGR} can be observed. Fig. 14 plots the crankshaft angle at which 50% of the mixture has already burned, i.e. *MFB50*, as a function of the *EGR*. The influence on the combustion duration results to be appreciable even for small *EGR* mass fractions and becomes more evident for higher X_{EGR} than 40%. *MFB50* is delayed for all the examined key-points, as X_{EGR} is augmented, since *EGR* slows the chemical reactions.

5. CRANKSHAFT BASED DIAGRAMS FOR THE MAIN IN-CYLINDER QUANTITIES.

Figures 15-24 report the unburned gas mass (M_u), the in-cylinder pressure (p_{cyl}), the *HRR*, the in-cylinder burned zone gas temperature (T_b), the NO_x and the soot as functions of the crankshaft angle. The p_{cyl} traces were acquired experimentally using 0.1° CA (crank angle degree) steps and were averaged over 100 consecutive engine cycles; the *HRR* was evaluated by means of a standard 1 zone diagnostic tool on the basis of the p_{cyl} distribution, while the histories of M_u, T_{cyl}, NO_x and soot were calculated by means of a three-zone diagnostic tool on the basis of the p_{cyl} data. The diagnostic model fitting coefficients were calibrated on the basis of the experimental engine-out emissions [42].

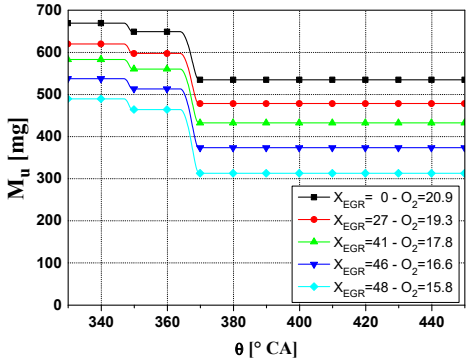

Figure 15. Unburned gas mass as a function of θ(2000x2).

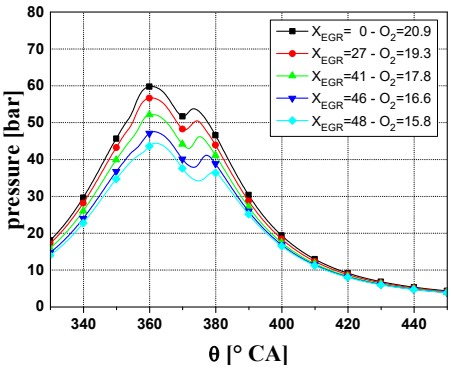

Figure 16. In-cylinder pressure as a function of θ(2000x2).

The unburned mass M_u accounts for the mixture that has not yet burned at the considered crank angle. Before injection has occurred, M_u is equal to the sum of the inlet fresh air, the *EGR* and the residual gas mass fraction from the previous cycle. As injection takes place, some fuel enters the combustion chamber and mixes with the unburned gases and, as a result, a mixture zone is formed, in which the mass ratio of the air to the fuel is approximately stoichiometric. The unburned mass progressively reduces during the injection and combustion period, as is shown in Fig. 15 for the 2000×2 key-point, since part of the initial M_u enters the model mixture zone [42]. The increase in the *EGR* rate makes the value of M_u at θ=330° CA decrease, due to a diminution in the inlet charge density (thermal throttling effect). This reduction in M_u with X_{EGR} determines a reduction in the in-cylinder pressure before combustion, and a more intense reduction

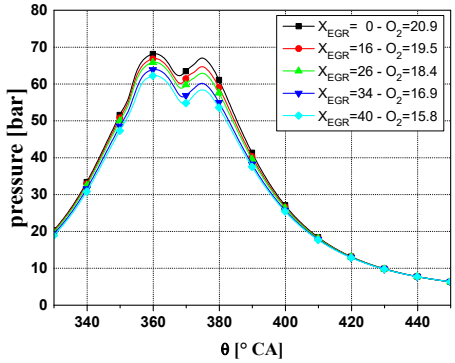

Figure 17. In-cylinder pressure as a function of θ(2000x5).

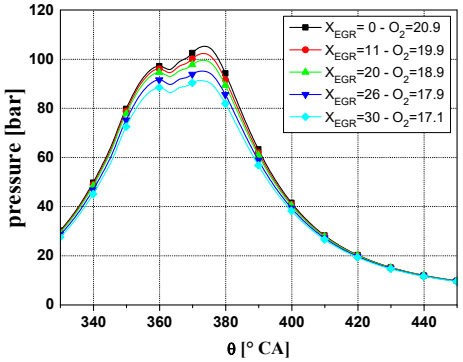

Figure 18. In-cylinder pressure as a function of θ(2500x8).

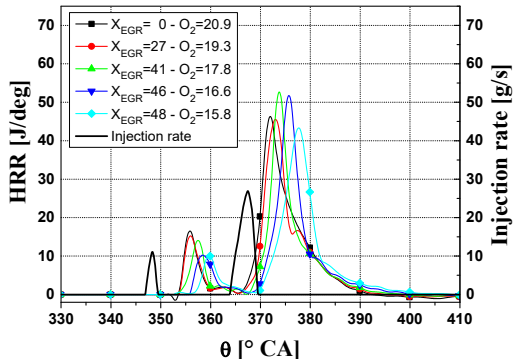

Figure 19. Heat release rate as a function of θ(2000x2).

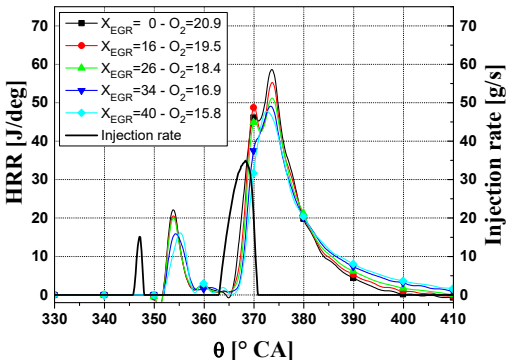

Figure 20. Heat release rate as a function of θ(2000x5).

during both the combustion and the early expansion phases (Fig. 16). Less influence of the *EGR* on p_{cyl} is detected as the engine load is increased (Figs. 17 and 18), because combustion is more vigorous and the smaller X_{EGR} values induce lower percentage variations of M_u.

The *HRR* (thin lines with symbols) and the injection rate (thick solid line) distributions versus the crankshaft angle have been plotted in Fig. 19 for the 2000×2 key-point. Just one injection rate pattern was plotted in order to avoid the overlapping of many curves, but also considering that the variation with *EGR* was minor. The first peak in the *HRR* is related to the pilot injection and is always lower than the second one, which refers to the main combustion. The various changes in the engine inlet charge composition and temperature, due to the *EGR* rate variations, generally alter the fuel mixing with air and the chemical reaction times, that is, the length of the ignition delay. In particular, the ignition delay, which is evaluated as the distance between the start of injection and the corresponding increase in the *HRR* of the pilot injection, tends to lengthen in Fig. 19 when X_{EGR} increases, because the dilution effect prevails over the opposing effect of the increase in the temperature of the inlet charge. However, it is also possible that the two opposite effects balance each other, and in these cases, the ignition delay remains almost unchanged with X_{EGR} [23].

The combustion mainly occurs in the premixed phase, as can be seen in Fig 19. In fact, when the combustion of the main injected fuel starts, most of the fuel has already been injected and has had enough time to mix with the in-cylinder charge according to a partial *PCCI* process. Although the increased fuel ignition delay, due to the higher X_{EGR}, leads to an increasing amount of fuel that burns in a premixed combustion phase, the reduction in oxygen availability decreases the rate at which the fuel burns in the premixed phase. The prevailing effect depends on the *EGR* rate value and on the considered injection shot (pilot or main).

In Fig. 19, it can be observed that, the *HRR* peak always decreases for the pilot injection, whereas the growth in the premixed fraction determines an increased and retarded main combustion *HRR* peak for X_{EGR} values of up to 40-45%, compared to the working condition without *EGR*. When X_{EGR} is increased beyond 45%, the effect of the deceleration of the chemical reaction kinetics prevails over the increased ignition delay and the main combustion *HRR* peak decreases with the *EGR* rate rise. As soon as the load increases, a larger fraction of the mixture burns in the mixing-controlled combustion phase. Furthermore, the ignition delay has been proved to be less sensitive (Fig. 20) or even insensitive to X_{EGR} (Fig. 21); in fact, the unburned gas temperature increases, the combustion reactions become faster and, therefore, the influence of the $[O_2]_{int}$ concentration on the ignition delay becomes marginal. However, the combustion velocity slows down as the *EGR* rate increases, and the intensity of the *HRR* peak that corresponds to the main injection continues to decrease as X_{EGR} rises for medium and high loads.

Figure 22 plots the in-cylinder *NO* volume fraction time history (*NO* represents most of the NO_x since NO_2 is minor) for the 2000×2 case. The *NO* time distribution was calculated using the extended Zeldovich model [41]. The NO_{end}/NO_{start}

ratio, where the subscripts *start* and *end* stand for the in-cylinder *NO* volume fraction before the start of combustion (evaluated at θ=330° CA) and after the end of combustion (evaluated at θ=450° CA), respectively, tends to decrease as X_{EGR} increases. The absolute value of NO_{start} is proportional to the product of the *EGR* mass and the NO_{end} concentration. When X_{EGR} increases, the *EGR* mass grows, while the fraction of *NO* in this mass, i.e. NO_{end}, decreases. As a result, the absolute value of NO_{start} first increases with X_{EGR} (e.g. from X_{EGR} = 0 to X_{EGR} = 27% in Fig. 22) and then decreases with it (e.g. from X_{EGR} = 41% to X_{EGR} = 48% in Fig. 22).

Figure 23 shows the temperature of the in-cylinder burned gases, which was calculated in the combustion chamber for different *EGR* mass fractions for the 2000×2 case. The *EGR* reduces the combustion peak temperatures of the burned gases and is responsible for the massive reduction in the *NO* concentration at the end of combustion (Fig. 22). The growth in the intake temperature, due to the increase in the *EGR* mass fraction, leads to slightly raised unburned gas temperatures during the compression phase. This behavior is not in conflict with the decreasing trend of NO_x with X_{EGR}, since the NO_x emissions are closely correlated to the peak temperature of the burned gas zone ($T_{bmax,main}$ around $\theta \approx 360°$ CA in Fig. 23) as well as to the residence time of the burned gases at higher temperatures than 1900-2000 K, but not to the average gas temperatures in the cylinder.

The soot formation and the soot oxidation phases are outlined in Figs. 24-26. Different engine soot emission trends, with respect to X_{EGR}, can be observed on the basis of the considered load. Soot formation depends on the local temperature and on $[O_2]_{int}$. The dilution effect of *EGR* has a reduced impact on $[O_2]_{int}$ at low loads (Fig. 24), because of the relatively high value of λ. On the other hand, an increased *EGR* mass determines a significant reduction in the burned gas temperature and a consequent reduction in both soot formation and oxidation. The former effect prevails over the latter, and the soot evaluated at $\theta \approx 450°$ CA results to reduce in Fig. 24 when X_{EGR} is increased. In other words, most of the fuel is burning under a premixed phase at low loads: fuel, fresh air and *EGR* are mixed thoroughly prior to combustion, local fuel-rich regions are reduced and combustion temperatures are decreased by *EGR*. On the other hand,

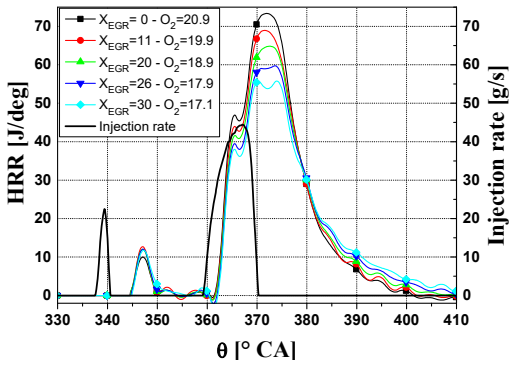

Figure 21. Heat release rate as a function of θ (2500x8).

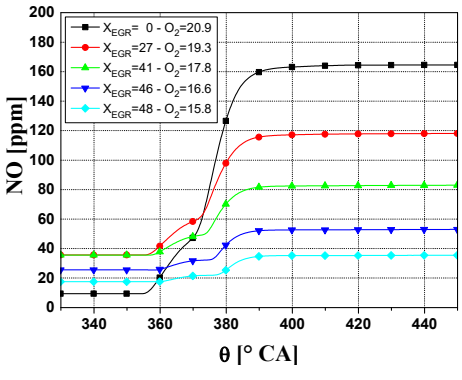

Figure 22. *NO* as a function of θ (2000x2).

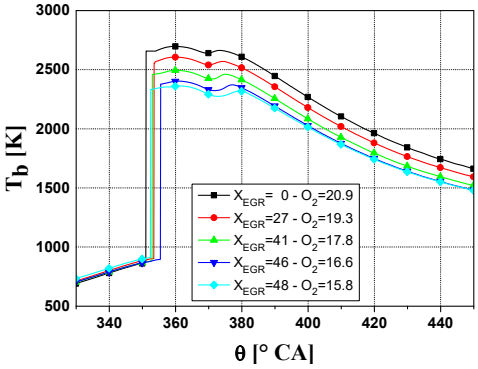

Figure 23. Burned gas temperature as a function of θ (2000x2).

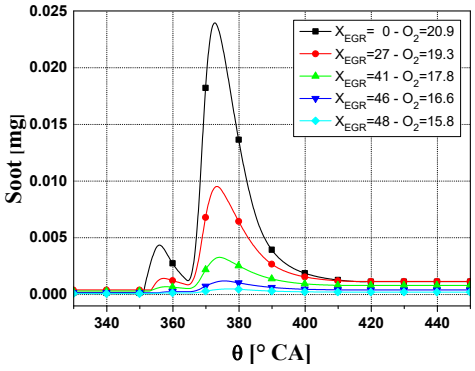

Figure 24. Soot as a function of θ (2000x2).

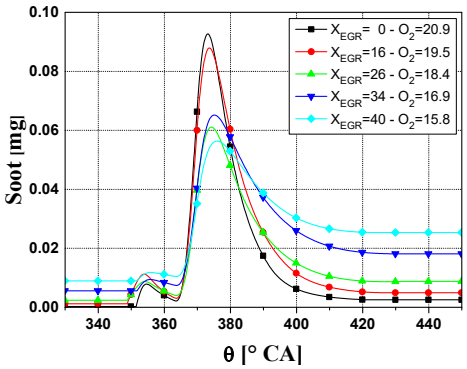

Figure 25. Soot as a function of θ (2000x5).

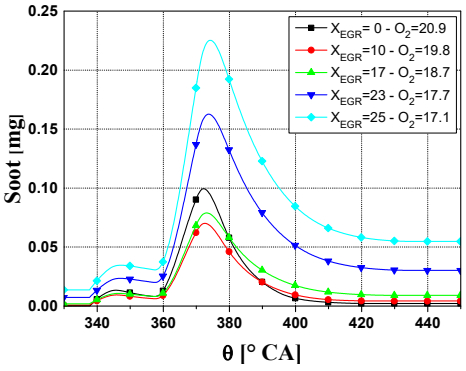

Figure 26. Soot as a function of θ (2750x12).

the soot levels observed in Fig. 24 at all the X_{EGR} values are generally not a reason for concern.

The soot formation rate for medium loads (*bmep* = 5 in Fig. 25), continues to reduce as the *EGR* rate is increased, but the oxidation rate becomes very low for high *EGR* rates, because of the reduced in-cylinder temperatures. The latter effect becomes the prevailing one in determining the fate of soot, which increases with X_{EGR} at the end of combustion. Finally, at high loads (*bmep* = 12 bar in Fig 26), the augment in X_{EGR} makes λ approach the stoichiometric value, and this effect prevails over the diminution of the burned gas temperatures, and leads to a significantly increased soot formation rate. The soot oxidation rate is negatively affected by *EGR* at high loads, as it is for the low and medium loads. In short, more soot is measured at the engine exhaust when X_{EGR} grows at high loads.

6. CONCLUSIONS.

The *EGR* mass fraction has been varied within the 0÷50% range at different steady-state key-points for an automotive Euro 5 low compression ratio diesel engine with an optimized pilot-main double injection strategy, managed with a late *PCCI* type combustion strategy. The selected key-points are representative of the engine application to a vehicle running the *NEDC*. The analysis has been performed considering both the time averaged quantities measured at the test bench and results derived from the application of diagnostic combustion models to the ensemble in-cylinder pressure time history. Attention has been paid to the benefits that high *EGR* rates can have on NO_x reduction and to any possible simultaneous detrimental effects. The largest range of *EGR* rates has been explored without finding an optimal value for

X_{EGR}, which is established as a trade-off between different engine-out emissions and brake specific fuel consumption, but also depends on the synergy between the combustion strategy and the installed aftertreatment devices.

The main achievements of the research investigation are synthetically listed hereafter:

- The ignition delay tends to increase at low loads as the EGR increases as a result of the reduction in the oxygen concentration because the EGR dilution effect prevails over the increase in the temperature of the inlet charge (thermal throttling effect). The ignition delay has been proved to be less sensitive or even insensitive to X_{EGR} at medium and high loads because the unburned gas temperature increases, the combustion reactions become faster and the influence of the $[O_2]_{int}$ concentration becomes marginal.
- The utilization of the *EGR* generally determines an almost linear decrease in λ when X_{EGR} increases. However, if high *EGR* rate values, which are typical of *PCCI* type engines, are applied at low loads, a deviation from linearity occurs, since the desired level of boost pressure that is set by the *ECU* cannot be maintained in the intake manifold. In fact, the high mass flow-rate, which is sent back from the exhaust to the intake manifold, determines an insufficient enthalpy flux to the turbine. Furthermore, fresh-air throttling reduces the pressure in the intake manifold.
- The NO_x emission data, referring to the different key-points, are more closely correlated to $[O_2]_{int}$ than to the maximum burned gas temperature. An almost quadratic monotonically increase in NO_x has been found with respect to $[O_2]_{int}$. The combustion timing of the main injection has also been confirmed to have a significant impact on reducing NO_x emissions. The best results, in terms of NO_x reduction, have therefore been achieved in late *PCCI* type strategies, when the combustion timing is retarded and high *EGR* rates are applied.
- The *HC* and *CO* emissions are relevant at low loads for partial *PCCI* engines subjected to heavy *EGR* rates, because fuel over-mixing and wall-quenching occur, due to the very lean mixture and the low temperatures. The influence of *EGR* on these emissions is not so significant, if *EGR* rates of up to 30-40% are applied, as occurs in conventional diesel combustion systems, and, in these conditions, *EGR* can even have a positive effect on *HC* emissions.
- Soot is sensitive to the *EGR* rate and increases exponentially with the *EGR* rate at medium and high conditions. The increase in soot with X_{EGR} is mainly due to the lack of oxygen in the recirculated exhaust gases. It is therefore difficult to employ high *EGR* rates at medium and high loads, due to diffusive combustion deterioration. Therefore, soot and NO_x show a trade-off behavior, with respect to X_{EGR}, at medium and high loads. On the other hand, heavy *EGR* rates allow NO_x and soot emissions to be improved simultaneously at low loads, because the low compression ratio engine works in partial *PCCI* mode.
- Brake specific fuel consumption is hardly affected by the *EGR* rate at medium and high loads. The influence of *EGR* on the *bsfc* for $bmep \geq 5$ bar does not show a definite trend up to $X_{EGR} \approx 20\%$. A small increase in *bsfc* can be

observed for higher *EGR* mass fractions than 20%, mainly due to the reduction in λ and to the longer duration of combustion. Instead, a decrease in *bsfc* can be found when passing from no *EGR* to around X_{EGR}≈30% at low loads. This is related to the combustion of the unburned hydrocarbons that enter the combustion chamber with the cooled *EGR*, which involves more O_2 at low loads than at higher loads and acts as a pre-heater of the intake mixture. However, *bsfc* increases with X_{EGR} for heavy *EGR* rates at low loads, due to a lack of fresh air, which is necessary to burn all the injected fuel, and this represents a drawback for the use of high *EGR* rates in *PCCI* strategies.

- The stability of the combustion is not affected significantly by the *EGR* rate: the coefficient of variation of the *imep* is always lower than 3% for all the considered *EGR* mass fractions. The increase in the *EGR* rate generally makes the combustion noise decrease, but the effectiveness of this measure depends on the engine load and on the *EGR* rate. An important reduction in *CN* occurs under heavy *EGR* rates for the *PCCI* working mode.

7. NOMENCLATURE

bmep	brake mean effective pressure
bsfc	brake specific fuel consumption
CA	crank angle
CN	combustion noise
COV_{imep}	coefficient of variation for the specific torque
$[CO_2]_{amb}$	volume concentration of CO_2 in the external environment
$[CO_2]_{exh}$	volume concentration of CO_2 in the engine exhaust
$[CO_2]_{int}$	volume concentration of CO_2 in the intake manifold
ECU	electronic control unit
EGR	exhaust gas recirculation
HC	unburned hydrocarbons
HCCI	homogeneous charge compression ignition
HRR	heat release rate
imep	indicated mean effective pressure
LTC	low-temperature combustion
$\dot{m}_a$	fresh air mass flow-rate
$\dot{m}_{EGR}$	exhaust gas mass flow-rate
M_u	unburned gas mass

420	*MFB50*	angle at which 50% of the combustion mixture has burned
421	n	engine speed
422	NO_{start}	*NO* emissions before the start of combustion
423	NO_{end}	*NO* emissions after the end of combustion
424	NO_x	nitrogen oxides
425	$[O_2]_{int}$	oxygen volume concentration in the intake manifold
426	p_{int}	pressure in the intake manifold (boost pressure)
427	p_{cyl}	in-cylinder pressure
428	*PCCI*	partial premixed charge compression ignition
429	*PM*	particulate matter
430	q_{pil}	volume of fuel injected in the pilot injection
431	SOI_{Main}	electrical start of the main injection
432	SOI_{Pil}	electrical start of the pilot injection
433	T_b	in-cylinder burned gas temperature
434	$T_{bmax,main}$	maximum in-cylinder burned gas temperature
435	*TDC*	top dead center
436	X_{EGR}	mass fraction of exhaust gas recirculation
437	ϕ	equivalence ratio
438	λ	relative air-fuel ratio
439	θ	crankshaft angle

440 8. REFERENCES.

441 [1] Zheng M, Reader GT, Hawley JG. Diesel engine exhaust gas recirculation—a review on advanced and novel
442 concepts. *Energy Conversion and Management*, 2004, vol. 45, pp. 883–900.

443 [2] Ladommatos N, Abdelhalim SM, Zhao H, Hu Z. Effects of EGR on Heat release in Diesel Combustion. SAE
444 Paper No. 980184.

445 [3] Pickett LM and Siebers DL. Non-Sooting Low Flame Temperature Mixing-Controlled DI Diesel Combustion.
446 SAE Paper No. 2004-01-1399

447 [4] Lapuerta M, Hernandez JJ, Gimenez F. Evaluation of exhaust gas recirculation as a technique for reducing diesel
448 engine NO_x emissions. *Proc Instn Mech Engrs part D J Autom Engns*, 2000, vol 214, pp. 85-93.

449 [5] Heywood JB. Internal Combustion Engine Fundamentals. New York, McGraw-Hill International Editions, 1988.

[6] Zelenka P, Aufinger H, Reczek W, Catellieri W. Cooled EGR—a key technology for future efficient HD Diesels. SAE Paper No. 980190.

[7] Kreso AM, Johnson JH, Gratz LD, Bagley ST, Leddy DG. A study of the effects of exhaust gas recirculation on heavy-duty Diesel engine emissions. SAE Paper No. 981422.

[8] Maiboom A, Tauzia X, Helet J. Experimental study of various effects of exhaust gas recirculation (EGR) on combustion and emissions of an automotive direct injection diesel engine, *Energy*, 2008, vol. 33, pp. 22-34..

[9] Abd-Alla GH., Using exhaust gas recirculation in internal combustion engines: a review, *Energy Conversion and Management*, 2002, vol. 43, pp. 1027–1042.

[10] Ladommatos N, Abdelhalim SM, Zhao H, Hu Z. The effects of carbon dioxide in exhaust gas recirculation on diesel engine emissions. *Proc Instn Mech Engrs part D J Autom Engns*, 1998, vol. 212, pp. 25-42.

[11] Agarwal D., Singh SK., Agarwal AK. Effect of Exhaust Gas Recirculation (EGR) on performance, emissions, deposits and durability of a constant speed compression ignition engine. *Applied Energy*, 2011, vol. 88, pp. 2900–2907.

[12] Hountalas DT, Mavropoulos GC, Binder KB. Effect of exhaust gas recirculation (EGR) temperature for various EGR rates on heavy duty DI diesel engine performance and emissions. *Energy*, 2008, vol. 33, pp. 272–283.

[13] Park, Y., and Bae, C., 2014. Experimental study on the effects of high/low pressure EGR proportion in a passenger car diesel engine. *Applied Energy*, 2014, vol.133, pp. 308-316.

[14] Reader GT, Galinsky G, Potter I, Gustafson RW. Combustion noise levels and frequency spectra in an IDI Diesel engine using modified intake mixtures. *Emerging Energy Technol Trans ASME*, 1995, vol.66, pp. 53–58.

[15] Kouremenos D. A., Hountalas D. T., Binder K. B., The Effect of EGR on the Performance and Pollutant Emissions of Heavy Duty Diesel Engines using Constant and Variable AFR, SAE Paper No. 2001-01-0198.

[16] McKinley TL. Modeling Sulfuric Acid Condensation in Diesel Engine EGR Coolers. SAE Paper No. 970636.

[17] Lim J, Kang B, Park J, Yeom Y, Chung S, Ha J. A Study on Exhaust Characteristics in HSDI Diesel Engine Using EGR Cooler. Proceedings of the KSAE 2004 Fall Conference, pp. 306–312.

[18] Schubiger R, Bertola A, Boulouchos K. Influence of EGR on Combustion and Exhaust Emissions of Heavy Duty DI-Diesel Engines equipped with Common-Rail Injection Systems. SAE Paper No. 2001-01-3497.

[19] Dennis AJ., Garrner CP., Taylor DHC. The Effect of EGR on Diesel Engine Wear. SAE Paper No. 1999-01-0839.

[20] Ishiki K, Oshida S, Takiguchi M. A study of abnormal wear in power cylinder of diesel engine with EGR-wear mechanism of soot contaminated in lubricating oil. SAE Paper No. 2000-01-0925.

[21] Agarwal AK, Singh SK, Sinha S, Shukla MK. Effect of EGR on the exhaust gas temperature and exhaust opacity in compression ignition engines. *Sadhana* Vol. 29, Part 3, June 2004, pp. 275–284.

[22] Ladommatos N, Abdelhalim SM, Zhao H, Hu Z. The Dilution, Chemical, and Thermal Effects of Exhaust Gas Recirculation on Diesel Engine Emissions - Part 4: Effects of Carbon Dioxide and Water Vapour. SAE Paper No. 971660.

[23] Jacobs T, Assanis D, Filipi Z. The Impact of Exhaust Gas Recirculation on Performance and Emissions of a Heavy-Duty Diesel Engine. SAE Paper No. 2003-01-1068.

[24] Wilson RP, Muir EB, Pellicciotti FA. Emissions study of a single-cylinder diesel engine, SAE paper No. 740123.

[25] Zhu Y, Ricart-Ugaz L, Wu S, Cigler J, El-Beshbeeshy M, Bulicz T, Yan J. Combustion Development of the New International 6.0L V8 Diesel Engine. SAE Paper No 2004-01-1404.

[26] Nitu B, Singh I, Zhong L, Badreshany K, Henein NA, Bryzik W. Effect of EGR on autoignition, combustion, regulated emissions, and ldehydes in DI diesel engines. SAE paper no. 2002-01-1153.

[27] Uchida N, Daisho Y, Saito T, Sugano H. Combined Effects of EGR and Supercharging on Diesel Combustion and Emissions. SAE Paper No. 930601.

[28] Park J, Song S, Lee KS. Numerical investigation of a dual-loop EGR split strategy using a split index and multi-objective Pareto optimization. *Applied Energy*, 2015, vol. 142, pp. 21-32.

[29] Verschaeren, R., Schaepdryver, W., Serruys, T., Bastiaen, M., Vervaeke, L., Verhelst, S. Experimental study of NO_x reduction on a medium speed heavy duty diesel engine by the application of EGR (exhaust gas recirculation) and Miller timing, *Energy*, 2014, vol. 76, pp. 614-621.

[30] Yao M, Zheng Z, Liu H. Progress and recent trends in homogeneous charge compression ignition (*HCCI*) engines. *Progress in Energy and Combustion Science*, 2009, vol. 35, pp. 398–437.

[31] Saxena S, Bedoya ID. Fundamental phenomena affecting low temperature combustion and HCCI engines, high load limits and strategies for extending these limits. *Progress in Energy and Combustion Science*, 2013, vol. 39, pp. 457-488, http://dx.doi.org/10.1016/j.pecs.2013.05.002.

[32] Fang Q, Fang J, Zhuang J, Huang., A. Influences of pilot injection and exhaust gas recirculation on combustion and emissions in a HCCI-DI combustion engine. *Applied Thermal Engineering*, 2012, vol. 48, pp. 97-104.

[33] Han D, Ickes AM, Bohac SV, Huang A, Assanis DN. HC and CO emissions of premixed low-temperature combustion fueled by blends of diesel and gasoline. *Fuel*, 2012, 99, pp. 13–19.

[34] Sethi VP, Salariya KS. Exhaust Analysis and Performance of a Single Cylinder Diesel Engine Run on Dual Fuels. *IE(I) Journal-MC*, vol 85, April 2004.

[35] L. Cornolti, A. Onorati, T. Cerri, G. Montenegro, F. Piscaglia. 1D simulation of a turbocharged Diesel engine with comparison of short and long EGR route solutions. *Applied Energy*, vol. 111, 2013, pp. 1-15.

[36] d'Ambrosio S, Ferrari A, Spessa E. Analysis of the Exhaust Gas Recirculation System Performance in Modern Diesel Engines. *Journal of Engineering for Gas Turbines and Power*, 2013, Vol. 135, pp. 0816011-08160113.

[37] R. Manimaran, R. Thundil Karuppa Raj, CFD Analysis of Combustion and Pollutant Formation Phenomena in a Direct Injection Diesel Engine at Different EGR Conditions, *Procedia Engineering*, 2013, vol. 64, pp. 497-506.

[38] Lee Y., Huh, K. Y. Analysis of different modes of low temperature combustion by ultra-high EGR and modulated kinetics in a heavy duty diesel engine. *Applied Thermal Engineering*, 2014, vol. 70 (1), pp. 776-787.

[39] Zheng, Z., Yue, L., Liu, H., Zhu, Y., Zhong, X., Yao, M. Effect of two-stage injection on combustion and emissions under high EGR rate on a diesel engine by fueling blends of diesel/gasoline, diesel/n-butanol, diesel/gasoline/n-butanol and pure diesel. *Energy Conversion and Management*, 2015, vol. 90, pp. 1-11

[40] d'Ambrosio S, Finesso R, Spessa E. Calculation Of Mass Emissions, Oxygen Mass Fraction And Thermal Capacity Of The Inducted Charge In SI And Diesel Engines From Exhaust And Intake Gas Analysis. *Fuel*, 2011, n. 90, issue 1, pp. 152-166.

[41] d'Ambrosio S., Finesso R., Fu L., Mittica A. and Spessa E., A control-oriented real-time semi-empirical model for the prediction of NOx emissions in diesel engines. *Applied Energy*, 2014, vol. 130, pp. 265–279.

[42] Finesso R, Spessa E. A real time zero-dimensional diagnostic model for the calculation of in-cylinder temperatures, HRR and nitrogen oxides in diesel engines. *Energy Convers Manage*, 2014, vol.79, pp. 498–510.

[43] Liu H, Li S., Zheng Z, Xu J, Yao M. Effects of n-butanol, 2-butanol, and methyl octynoate addition to diesel fuel on combustion and emissions over a wide range of exhaust gas recirculation (EGR) rates. *Applied Energy*, 2013, vol. 112, pp. 246–256

[44] Zamboni, G., Capobianco, M. Influence of high and low pressure EGR and VGT control on in-cylinder pressure diagrams and rate of heat release in an automotive turbocharged diesel engine. *Applied Thermal Engineering*, 2013, vol. 51 (1–2), pp. 586-596.